International Journal of Nanomedicine

Dovepress

open access to scientific and medical research

Open Access Full Text Article

ORIGINAL RESEARCH

Echogenic PEGylated PEI-Loaded Microbubble As Efficient Gene Delivery System

This article was published in the following Dove Press journal:
International Journal of Nanomedicine

Chun Liufu[1]
Yue Li[1]
Jiawei Tu[1]
Hui Zhang[1]
Jinsui Yu[1]
Yi Wang[1]
Pintong Huang[2]
Zhiyi Chen[1]

[1]Department of Ultrasound Medicine, Laboratory of Ultrasound Molecular Imaging, The Third Affiliated Hospital of Guangzhou Medical University, Experimental Center, The Liwan Hospital of The Third Affiliated Hospital of Guangzhou Medical University, Guangzhou, Guangdong 510000, People's Republic of China; [2]Department of Ultrasound, Second Affiliated Hospital, Zhejiang University School of Medicine, Hangzhou, Zhejiang Province, People's Republic of China

Background: Cancer stem cells (CSCs) are responsible for cancer therapeutic resistance and metastasis. To date, in addition to surgery, chemotherapy, and radiotherapy, gene delivery has emerged as a potential therapeutic modality for ovarian cancer. Efficient and safe targeted gene delivery is complicated due to the tumor heterogeneity barrier. Ultrasound (US)-stimulated microbubbles (MBs) have demonstrated a method of enabling non-invasive targeted gene delivery.

Purpose: The purpose of our study was to show the utility of poly(ethylene glycol)-SS-polyethylenimine-loaded microbubbles (PSP@MB) as an ultrasound theranostic and redox-responsive agent in a gene delivery system.

Patients and methods: PSP nanoparticles were conjugated to the MB surface through biotin–avidin linkage, increasing the gene-loading efficiency of MB. The significant increase in the release of genes from the PSP@MB complexes was achieved upon ultrasound exposure. The positive surface charge in PSP@MB can condense the plasmid through electrostatic interactions; agarose-gel electrophoresis further confirmed the ability of PSP@MB to condense plasmids. The morphology, particle sizes and zeta potential of PSP@MB were characterized by transmission electron microscopy and dynamic light scattering.

Results: Laser confocal microscopy showed that the combination of ultrasound with PSP@MB could promote the cellular uptake of plasmids. Plasmids which encode enhanced green fluorescence protein (EGFP) reporter genes or luciferase reporter genes were delivered to CSCs in vitro and to subcutaneous xenografts in vivo via the combination of ultrasound with PSP@MB. Gene transfection efficiency was evaluated by fluorescence microscopy and In Vivo Imaging Systems. This study demonstrated that the combination of ultrasound with PSP@MB can remarkably promote gene delivery to solid tumors as well as diminishing the toxicity towards normal tissues in vivo. The combination of PSP@MB and the use of ultrasound can efficiently enhance accumulation, extravasation and penetration into solid tumors.

Conclusion: Taken together, our study showed that this novel PSP@MB and ultrasound-mediated gene delivery system could efficiently target CSCs.

Keywords: ultrasound, PEGylated PEI-loaded microbubble, cancer stem cell, gene delivery

Introduction

Ovarian tumors are phenotypically heterogeneous and include subpopulations of cancer stem cells, which exhibit a significant obstacle toward solid tumor treatment.[1] Routine chemotherapy and radiotherapy are mainly to kill mitotic phase cancer cells, not including CSC.[2,3] CSC are regarded as a key point in the origin of tumor relapse and chemo-resistance due to the its characteristic property, such as slow cell cycle, self-renewal capabilities, differentiation and tumorigenesis in vivo.[4,5]

Correspondence: Zhiyi Chen
Department of Ultrasound Medicine, Laboratory of Ultrasound Molecular Imaging, The Third Affiliated Hospital of Guangzhou Medical University, Guangzhou 510150, People's Republic of China,
Tel +86-020-81292115
Email winchen@vip.126.com

submit your manuscript | www.dovepress.com
DovePress
http://doi.org/10.2147/IJN.S217338

Gene therapy is a promising strategy for reducing the risks of cancer relapse and metastasis. Cationic polymer nanoparticles (NPs) have been investigated as non-viral vectors for gene delivery due to their favorable safety profile when compared to viral vectors. Vaidyanathan et al summarized that there were five possible rate-limiting processes involved in gene delivery: (i) protection of DNA from nucleases, (ii) transport within specific intracellular pathways, (iii) endosomal release, (iv) transport into the nucleus, and (v) DNA release from vectors.[6] In most cases, there were different demands for the attributes of NPs in different phases during the delivery process to solid tumor in vivo. Low positive charges or negative charges were conducive to the stability of NPs during circulation; however, high positive charges were required for a higher cancer cellular uptake.[7] Among the non-viral gene vectors, high-molecular weight polyethylenimines (PEIs) are widely used for in vitro gene transfection. In our previous experiments, we showed that gene transfection efficiency was enhanced by low-dose 25 kDa-branched PEI with the assistance of 1.8 kDa-branched PEI with low cytotoxicity in vitro.[8] To overcome these obstructions, many researches have modified the surface of polymer nanoparticles to achieve safer and more efficient gene delivery. According to the characteristics of the tumor microenvironment which involves acidity and a high concentration of glutathione (GSH), a gene delivery system capable of being triggered by pH or GSH must be designed. Guan et al showed that modified PEI was the result of polyethylene glycol (PEG) via the Schiff base reaction. PEGylation can shield the positive charges on the surface of PEIs and tighten the complex particles, leading to decreased cytotoxicity, improved stability and prolonged circulation. PEG shielding will rapidly disappear due to the acidic pH as soon as arriving at the tumor.[7] Other groups carried out similar studies. Luo and Lei demonstrated that nanoparticles which consisted of PEG-modified 25 kDa PEI via disulfide bonds (SS) had high transfection rates in vitro and in vivo. PEG shielding will also rapidly disappear due to GSH as soon as arriving at the tumor. Consequently, PEI/DNA nanoparticles can be taken up into cancer cells and escape from endosomes into the cytoplasm, then genes can be release without severe cytotoxicity.[9,10]

Several strategies are being explored to improve the therapeutic effect, by improving the delivery and accumulation of NPs in cancer tissue.[11,12] The use of therapeutic ultrasound has received great interest for the past two decades. Ultrasound-targeted gene delivery techniques show great potential to locally enhance NPs extravasation from the vascular system, penetration through the extracellular matrix and uptake into solid tumors.[13] In previous studies, De Cook et al compared the cellular delivery between nanoparticle-loaded MBs and unloaded MBs, and the experiments showed that the nanoparticle-loaded MBs substantially improved the cellular delivery of nanoparticles, whereas unloaded MBs did not enhance cellular delivery. There are different cell uptake mechanisms at different acoustic pressures: at low acoustic pressures endocytosis is enhanced, while higher acoustic pressures favored uptake via membrane pores. The new mechanism of "sonoprinting" was mentioned in the process of real-time swept field confocal microscopy imaging.[14] In our previous studies, Li et al showed that ultrasound increased the transfection rate of folate-modified chitosan nanoparticles/plasmid into 293T cells.[15]

De Cook et al had also shown that there were some definite advantages to the loading of nanoparticles onto MBs with biotin-avidin bridging. Firstly, the nanoparticle-loaded MBs can be tracked in the blood circulation in vivo by contrast-enhanced ultrasound. Secondly, focused ultrasound insonation enabled the nanoparticle-loaded MBs to form a passive targeting gene delivery system, which ensures that the attached nanoparticles are present at the target site. Thirdly, using the ultrasound-targeted MBs method at a targeted location leads to the targeted deposition of PSP nanoparticles and plasmid DNA (pDNA). Fourthly, the radiation force generated by focused ultrasound can increase the concentration of PSP nanoparticle-loaded MBs at the desired site.[14]

Effective delivery requires the PSP nanoparticles to be loaded onto the MBs. There are multiple methods to link the nanoparticles with the MBs. One of the most common methods to attach a nanoparticle to the MBs are through biotin-avidin interaction, which is one of the strongest non-covalent interactions in nature. This is because the avidin-biotin interaction possesses many innate advantages of simple fabrication without changing the biology and chemical properties of the coupled complexes. Therefore, the avidin-biotin interaction has been extensively utilized as probes and affinity matrices within various fields of nanotechnology, such as diagnostics, biochemical assays, tissue engineering and nanoscale delivery systems, including nucleic acids, vaccines, small molecules and so on.[16] Hence, in this article, the avidin-biotin interaction was applied to link the biotinylated PSP and the lipid biotinylated MB.

In this article, the ultrasound-triggered and GSH-sensitive gene release platform PSP@MB was produced successfully. The resulting PSP@MB was characterized by dynamic light scattering and transmission electron microscopy. There was a synergistic effect on gene transfection from the combination of ultrasound and PSP@MB in vitro and in vivo, indicating the potential application of this method for spatiotemporally-controlled gene delivery (Figure 1).

Materials And Methods

Materials

The phospholipids 1,2-dipalmitoyl-sn-glycero-3-phosphocholine (DPPC, MW, 734.039 g/mol) and 1,2-dipalmitoyl-3-trimethylammonium-propane (DPTAP) were purchased from Avanti Polar Lipids in USA. The phospholipids 1,2-distearoyl-sn-glycero-3-phosphoethanolamine-N-[methoxy (poly(ethyleneglycol))-2000] (DSPE-PEG2000-Biotin, MW, 3,016.781 g/mol) and Biotin-PEG(2k)-SS-NHS were purchased from Xi'an Ruixi Biological Technology Co. in China. Perfluoropropane (C_3F_8) gas was purchased from the R&D Center for Specialty Gases at the Research Institute of Physical and Chemical Engineering of Nuclear Industry (Beijing, China). FITC-Avidin was purchased from Solarbio Inc (Beijing, China). The human ovarian cancer cells A2780 were from the American Type Culture Collection.

Preparation Of PSP@MB Transfection Agent And DNA Binding Analysis

The lipid biotinylated MBs were synthesized by the thin-film hydration method. DPPC: DPTAP: DSPE-PEG2000-Biotin=9: 2: 1 were dissolved in 1 mL chloroform and drained to form a dried film by rotary evaporator for 24 h. The film was then hydrated with 0.2% glycerol phosphate-buffered saline (PBS). and the gas in the vial was replaced with C_3F_8. Finally, the vial was mechanically shaken for 45 s using agitator (TD-1002).

The biotin-PEG2000-SS-NHS and 25 kDa PEI were added together with a mass ratio of 1.25:1. It was then mixed on the magnetic stirrer overnight and put on dialysis for 24 hrs with a 3500 Da molecular weight cut-off. Then we used a 0.22 μm filter for sterilization and finally acquired sterile biotinylated PSP. The preparation of biotinylated PSP@ biotinylated MB complex was performed via the biotin–streptavidin bridging chemistry method. To start, the final concentration of 0.3 mg/mL of FITC-Avidin and the 10^{10} MBs/mL biotinylated MB was mixed with a volume ratio 1:1 and incubated for 30 min. The mixture was then washed three times with double-distilled water to remove unreacted avidin, centrifuged at 800 rcf for 5 min each time, before the upper foam was collected. Then we acquired avidin-MB. Next, 800 μL of biotinylated PSP was mixed with a volume ratio 10:1 and incubated for 30 min. The complexes were washed and centrifuged three times to remove the remainder of the unloaded biotinylated PSPs. Then the diameter, zeta-potential and concentration of the PSP@MB was characterized with ZS Nano (Malvern, UK) and Multisizer 3 (BECKMAN COULTER, USA), and used the fluorescence microscope to verify the connection of PSP@MB.[17,18]

The pDNA binding capability of was investigated by agarose gel electrophoresis. The PSP@MB/pDNA polyplexes were loaded into 0.7% agarose gel. The electrophoresis was run using TAE buffer at 100 V for 30 min. The gel was visualized stained by DNA dyes and analyzed under an electrophoresis gel imaging system.

Cell Culture

Human ovarian cancer cells lines A2780 were from the American Type Culture Collection (Rockville, MD, USA). The A2780 cells were cultured on ultra-low-attachment culture dishes (Corning). DMEM/F12 (Gibco) supplemented with 10 ng/mL bFGF (Invitrogen), 20 ng/mL EGF (PEPROTECT), Glutamax™-1 (100X, Gibco), sodium pyruvate (100X, Gibco), B27 (50X, Gibco), penicillin/streptomycin (100X), 20 mmol/L Y27632 (Wako), and 10 mg/mL insulin (Roche) were put in the culture dishes. For serial passage, spheroid cells were divided with TrypLE™ Express (Stem Cell Technologies Inc.) once every 7 days.[19]

ALDEFLUOR Assay And Fluorescence-Activated Cell Sorting

The enzymatic activity of aldehyde dehydrogenase1 (ALDH1) within the ovarian carcinoma A2780 cell suspensions were measured using the ALDEFLUOR Stem Cell Identification Kit (Stem Cell Technologies, Canada). The A2780 spheroid single cells were resuspended in Aldefluor assay buffer and incubated for 40 min at 37 ℃. The test ALDH1-positive population was gated using control cells incubated under identical condition in the presence of a 10-fold molar excess of the ALDH inhibitor, diethylamino benzaldehyde (DEAB). Fluorescence-Activated Cell Sorting

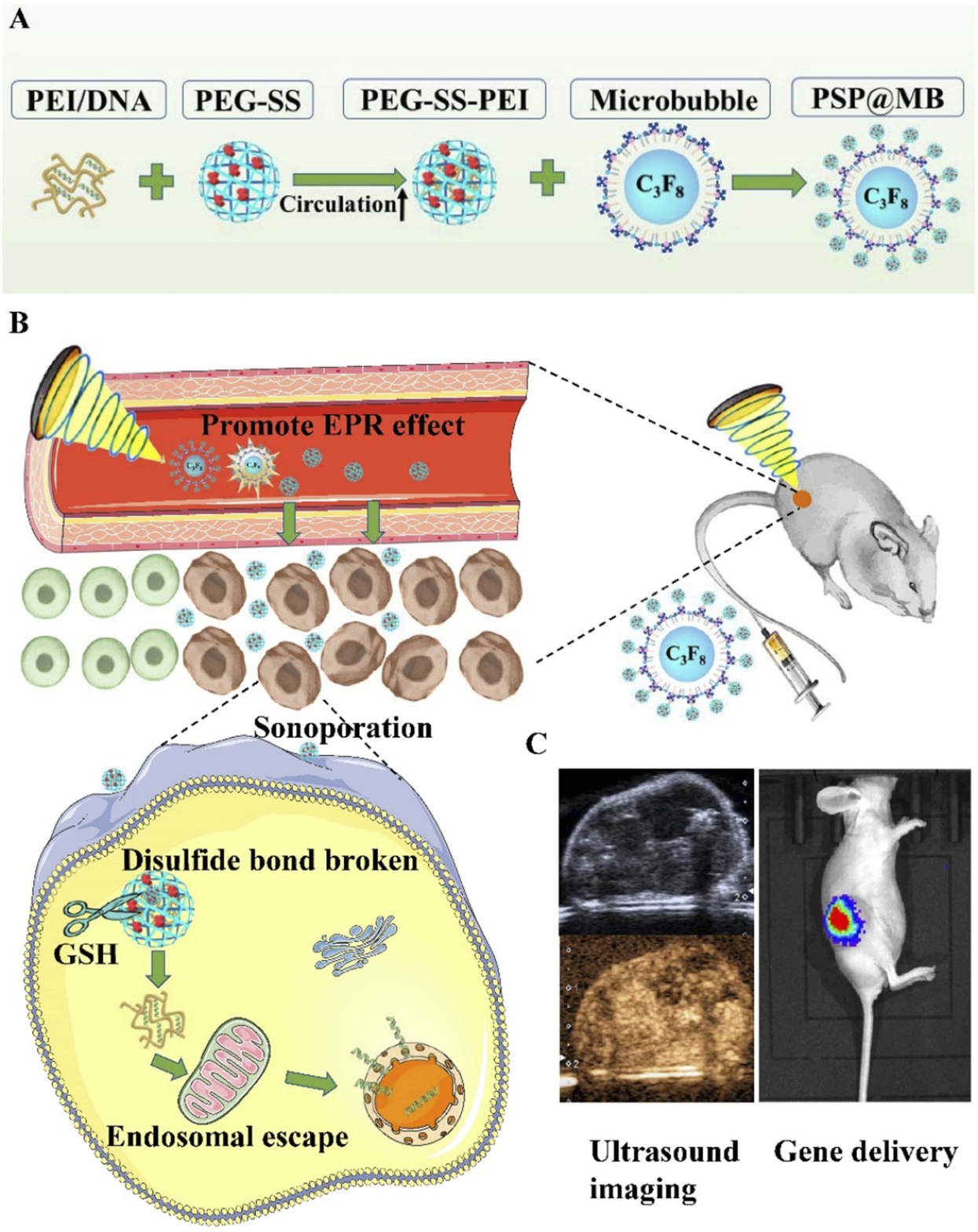

Figure 1 Graphical abstract.

Notes: (**A**) Schematic illustration of the construction of PSP@MB. (**B**) The combination of PSP@MB, and the use of ultrasound can efficiently promote the effect of EPR and enhance accumulation, extravasation and penetration into solid tumors. As soon as PSP@MB arrived at the tumor, PEG shielding will be rapidly cleaved by the abundance of GSH at the tumor site. Consequently, PEI/DNA nanoparticles can be internalized into cancer cells by sonoporation and endosomal escape in the cytoplasm, then finally DNA is released. (**C**) Gene delivery was evaluated by ultrasound imaging and In Vivo Imaging Systems.

Abbreviations: PEI, polyethylenimine; PEG, Polyethylene glycol; SS, disulfide bond; MB, microbubble; EPR, enhanced permeability and retention effect; GSH, glutathione.

(FACS) was performed with 1×10^6 cells using the BD FACS Aria III (Becton Dickinson, USA) under low pressure in the absence of UV light. FACS data were analyzed using BD FACS Diva software V6.1.3. After cell sorting, the $ALDH1^+$ cells and the $ALDH1^-$ cells were collected.[20]

Subcutaneous Ovarian Xenograft Model

Four-to-five weeks old female BALB/c-nu/nu mice weighing between 13–15 g were purchased from Guangdong Experimental Animal Center (qualification number SCXK (Guangdong)2013-0002). According to the rules of Committee on Animal Research and Ethics, this research project had been reviewed and approved to be appropriate and humane by Institutional Animal Care and Use Committee of Guangzhou Medical University. $ALDH1^+$ ovarian cancer stem cells (OCSCs) and $ALDH1^-$ A2780 cells were digested into a single cell suspension. 1×10^3 100 μL $ALDH1^+$ OCSCs and 100 μL Matrigel (Corning, USA) were mixed and injected into the right flank of each nude mouse (n=3, respectively). Feeding was continued under specific pathogen free (SPF) conditions, and the tumor volume was calculated as $L*W^2/2$; where L is length and W is width.

Cell Viability Assay

A CCK-8 assay was applied to evaluate the cell viability after co-incubation with PSP@MB for 24 hrs. The OCSCs and vascular endothelial cells (VECs) were seeded onto 96-well plates at 3,000 cells per well and cultured for 24 hrs. The experimental groups were similar to those described above. Transfection was conducted with 90 μL medium and 10 μL sample suspension by using the same process as previously described. All assays were performed in four replicates. Then, the plate was incubated for four hours. The absorbance at 450 nm in each well was measured by the Infinite F200 Multimode plate reader. Cell viability = (A1-A2)/(A3-A2) ×100%, where A1 is the absorbance of wells in the experimental group, A2 is the absorbance of wells containing medium and CCK-8 solution without cells and samples, and A3 is the absorbance of wells containing medium, CCK-8 solution, and cells without experimental samples.

Intracellular Uptake Of PSP@MB/pDNA In OCSCs Under Ultrasound

The characteristics of ultrasound combined with PSP@MB is that it facilitates sonoporation (the transient small pores of cell membrane), which facilitate entry of pDNA into cells. The scanning electron microscope (SEM) (HITACHI S-3700N, Japan) was used to observe the sonoporation of OCSCs under PSP@MB and ultrasound. Ultrasound parameters were (0.4 W/cm^2, 0.8 W/cm^2, 1.2 W/cm^2 of intensity, 1 MHz, 20% duty cycle, 1 min). The OCSCs sample were fixed by 3% glutaraldehyde for SEM imaging after 10 min of ultrasound exposure.

To find out the effects of pDNA cellar uptake of OCSCs after ultrasound exposure, OCSC spheres were blown into serum-free medium at a final concentration of 10^6 cells/mL. FITC-streptavidin was conjugated with MB, and the Cy5-labeled pDNA was loaded with PSP nanoparticles at a final concentration of 1 μM. Then, the PSP@MB/pDNA was observed with a confocal laser scanning microscope (CLSM) (Nikon, Japan). It was then mixed at room temperature by shaking gently for 15 mins. The optimal ultrasound parameters (0.8 W/cm^2, 1 MHz, 20% duty cycle, 1 min) were used for sonication. After sonication, 300μL OCSC samples were fixed at different time intervals (10 min, 60 min, 3 hrs, 20 hrs) by mixing with 4% paraformaldehyde. The samples were then washed with 2 mL PBS per plate and centrifuged at 1000 rpm for 5 min, twice. The samples were finally quenched with a sealing agent including DAPI and observed using a CLSM.

Transfection Efficiency Of OCSCs Via Ultrasound And PSP@MB In Vitro

After a series of characterization analysis about OCSCs and the gene vector PSP@MB, we used the gene vector PSP@MB to deliver the pDNA with our independent research ultrasonic transfection apparatus, SXULTRASONIC (Shengxiang Hi-Tech, CO., LTD., Shenzhen.) at different parameters, such as intensity (0.4~1 W/cm^2), duty cycle (20%), irradiation time (30 s~1 min), and PSP@MB concentration (2%). The optimized N/P ratio of pDNA was selected and the parameters of optimum ultrasound transfection (1 MHz, 20% and 0.8 W/cm^2, 1 min) was chosen. Ultrasonic irradiation was performed on the form of suspension cells (cell density of 1×10^7 cells/mL). In this experiment, we allocated six groups: (a) Control (plasmid), (b) PSP, (c) MB+US, (d) Lipofectamine 2000, (e) Lipofectamine 3000, (f) PSP@MB+US. PSP@MB and pDNA were mixed for 20 mins. The OCSCs were shifted into 15 mL centrifuge tubes and left to stand for 5 mins, and then we collected the sediment of OCSC spheres. The spheres were blown off gently with OptiMEM. 300 μL cell suspension, 10 μL PSP@MB and pDNA (30 μg) was inserted into each of

the 24 pore plates. The mixture was exchanged after 4 hrs. After 24 h the fluorescence intensity of the EGFP of OCSCs was observed with a fluorescence microscope and quantified using flow cytometry.

Flow Cytometry

After 24 h after treatment of ultrasound and PSP@MB, the OCSCs were collected with centrifugation for 5 min at 1,000 rpm (180 g) at 4°C. Then OCSCs pellet was resuspended in phosphate buffered saline (PBS) at a concentration of 1×10^6 cells/mL for analysis by flow cytometry. The percentage of transfected cells (EGFP expressing) in each sample was determined by the Flow Cytometry Facility (Life Technologies Attune NxT, Life Technologies, USA). The flow cytometer parameters were (the excitation at 488 nm, emission at 525 nm). The mean fluorescence intensity was recorded with 10.000 events per each sample.

Contrast-Enhanced Ultrasonography With PSP@MB In The Subcutaneous Xenograft

To assess the instantaneous biodistribution of PSP@MB in vivo, we performed ultrasonography on tumor-bearing BALB/c-nu/nu mice. Mice were anesthetized with pentobarbital 200 μL via intraperitoneal injection. In vivo imaging of the MBs was performed using Aplio 500 ultrasound (Toshiba, Japan) with an 18 MHz probe (MS250) allowing non-linear imaging. The gel pad was covered onto the subcutaneous tumor of mice; the probe was fixed and placed in the axial plane to image the whole subcutaneous tumor. Images were acquired using contrast mode acquisition. PSP@MB was injected at a concentration of 100 μL PSP@MB ($1.0\sim3.0\times10^{10}$ MBs/mL). The contrast-enhanced ultrasonography in subcutaneous xenograft lasted for more than 3 mins.

Exposure On The Low Intensity Focused Ultrasound (LIFU)

Gene delivery was performed using the ultrasound signal generator (AFG3000C, Tektronix) with a high-power amplifier (LZY-22+) and 1 MHz pulse focus probe. The system allowed the generation of any duty cycle and a peak negative pressure of 0.7 MPa at its focal zone (20 mm). The collimator was linked to the focus probe while the emission diagram of the system was provided by the ultrasound signal generator. The collimator (a 2 cm funnel-shaped spacer consisting of a rigid tube filled with de-aerated water) was used to ensure that the focal zone was located below the skin, in the subcutaneous xenografts of nude mice. The sonication probe was positioned on the right flank of the nude mice. PSP@MB injections were tested to determine optimal transfection conditions. The optimal ultrasound parameters were: 250mV voltage (acoustic pressure 0.7 MPa, measured with needle hydrophone and oscilloscope), 1 MHz, 10,000 cycles, and a pulse repetition frequency (PRF) of 5 Hz. The optimal sonoporation parameters were used to compare PSP, MB and PSP@MB gene carriers for plasmid luciferase reporter genes (n=3). PSP, MB and PSP@MB/plasmid luciferase complexes were prepared prior to injection in the tail vein with a PSP@MB at a concentration of 100 μL PSP@MB ($1.0\sim3.0\times10^{10}$ MBs/mL) and 80 μg (100 μL) of plasmid luciferase. The focus probe was exposed for 5 mins.

Bioluminescence Imaging

Luciferase expression was followed by bioluminescence imaging at 24 hrs, 48 hrs, 3 days, 4 days, and 5 days after exposure to the focused ultrasound. Firstly, mice were anesthetized with 3% isoflurane (Isovet, Virbac, France) in air for induction, and maintained at 1.5% isoflurane for imaging. Secondly, intraperitoneal injection of 150 mg/kg of luciferin (Xenolight D luciferin potassium salt, Perkin Elmer) was administered 5 min before image acquisition. Bioluminescence data was acquired with IVIS Lumina HTX (PerkinElmer, USA) at 10 min, placing 2 animals simultaneously in the device. This real-time bioluminescence imaging allowed the detection of the plateau of photon emission for each individual mouse. This time frame was used to calculate the photon emission (ph/s/cm^2/sr) within a constant pre-defined ellipsoid region of interest; followed by the placing of subcutaneous xenografts on each nude mouse. Statistical analysis of bioluminescence activity was performed with GraphPad Prism software (version 7.0, GraphPad Software, San Diego, CA, USA) using a non-parametric Mann–Whitney test between 2 groups. Differences were considered statistically significant for a p-value <0.05.

Biosafety Evaluation

To evaluate the biocompatibility of PSP@MB, histological examination of hematoxylin and eosin (H&E) staining of vital organs (heart, liver, spleen, lung, kidney) was carried out. Firstly, the mice were then sacrificed under deep anesthesia, and tissues were collected, fixed in 4% paraformaldehyde and processed for paraffin embedding. Sectioned paraffin blocks of tumors and the major organs (heart, liver, spleen, lung, kidney) were stained with

hematoxylin and eosin (H&E), and whole slide scanning was performed with inverted microscope (Olympus, Japan). Two pathologists of the pathology department of the Third Affiliated Hospital of Guangzhou Medical University (Guangzhou, China) performed the histopathological diagnosis of H&E staining sections.

To evaluate the biocompatibility of PSP@MB in vivo, whole blood and blood serums were collected from the retro-orbital plexus of each nude mouse under deep anesthesia at 48 h after intravenous injection of PSP@MB or lipofectamine 3000. The liver functions serum glutamic-pyruvic transaminase (ALT) and glutamic-oxalacetic transaminase (AST), renal functions (Crea, Urea and UA), Direct Bilirubin (D BILI) and routine blood parameters (hemoglobin and white blood cell) were tested at the clinical laboratory of the Third Affiliated Hospital of Guangzhou Medical University (Guangzhou, China).

Statistical Analysis

All experiments were performed at least three times each and the data were shown as the mean ± standard deviation (SD). One-way analysis of variance (ANOVA) was used to analyze the results. GraphPad Prism 6.0 (GraphPad Software Inc, San Diego, CA, USA) was used to obtain graphs and statistics. Significant values were designated as follows: $*P<0.05$, $**P<0.01$, and $***P<0.001$.

Results

Synthesis And Characterization Of The PSP NPs

Figure S1A showed the chemical structure diagram of PEI, PEG-SS-NHS and PSP. Biotinylated PSP was constructed by the PEI and biotin-PEG-SS-NHS via amide linkages (Figure S1A). The successful synthesis of PSP confirmed by ^{1}H NMR spectra of PSP in D_2O as shown in Figure 2C. The signals of PEG (3.65 ppm) in "a" and PEI (2.3–2.7 ppm) in "b" were found in the ^{1}H NMR spectra of PSP in D_2O (Figure 2C). The characterizations of PSP NPs are shown in Figure 2. The dynamic light scattering (DLS) measurement indicated that the average diameters of the PSP NPs were approximately 100 nm and showed a slight positive zeta potential of 4±2.5 mV due to the PEGylation (Figure 2A and B). To evaluate the reduction sensitivity, the PSP NPs were incubated with 10 mM GSH for 2 h. After the GSH treatment, the PSP NPs increased in size from 100±53 nm to 210±101 nm (Figure 2A) and showed a change in the surface charge from 4±2.5 mV to 12±4.3 mV (Figure 2B).

pDNA Binding Ability Of PSP NPs Analysis

The complexation of pDNA with PSP NPs is due to electrostatic neutralization. To confirm the pDNA binding ability of PSP NPs, we checked the retardation of pDNA mobility in agarose-gel electrophoresis. As shown in Figure 2D, the pDNA condensation ability of PSP NPs were tested with various N/P ratios (0, 8, 10, 11, 12, 14, 16). PSP showed beneficial complexation of pDNA. The pDNA were completely retarded at an N:P ratio of 16, which indicated that the PSP can complex the pDNA entirely. However, the optimized proportion for gene transfection between PSP@MB and pDNA complex is not just the N:P ratio of PSP/pDNA, but more important is the concentration of PSP@MB.

Synthesis And Characterization Of The MB And PSP@MB

To load the biotinylated PSP NPs with biotinylated lipid MBs, biotin-avidin method was used (Figure S1B). For this, DSPE-PEG-biotin functionalized lipids were incorporated in the MB shell. The biotinylated MBs were composited with the thin-film hydration method. FITC-streptavidin was conjugated with PSP NPs and MBs. Microscope image of PSP@MB was showed in Figure 2E. Fluorescence microscope confirmed successful connection of PSP loaded MBs (Figure 2F). The DLS measurement showed that the average diameters of the MBs and PSP@MB were approximately 495±132 nm and 502±75 nm (Figure 2J), and zeta potential were 7±3.6 mV and 13±4.4 mV (Figure 2I). Transmission electron microscope (TEM) images of MB and PSP@MB showed the similar particle size with DLS (Figure 2G and H).

Formation And Characterization Of OCSC Spheres Derived From A2780

The human ovarian cancer cell lines A2780 were cultured as monolayers and spheroids with serum or serum-free culture mediums. The spheroids were rich with a serum-free culture medium from the addition of the ROCK inhibitor Y27632, bFGF, EGF and insulin. The spheroids are shown in the first week and the third week (Figure S2A). Another method for enriching the spheroids was also used with cisplatin at a final concentration of 0.5 mg/mL for 24 h in the first week. It was motivating to discover that the spheroids were formed three weeks later with 0.5 mg/mL of cisplatin. ALDEFLUOR^{TM} assay and flow cytometry

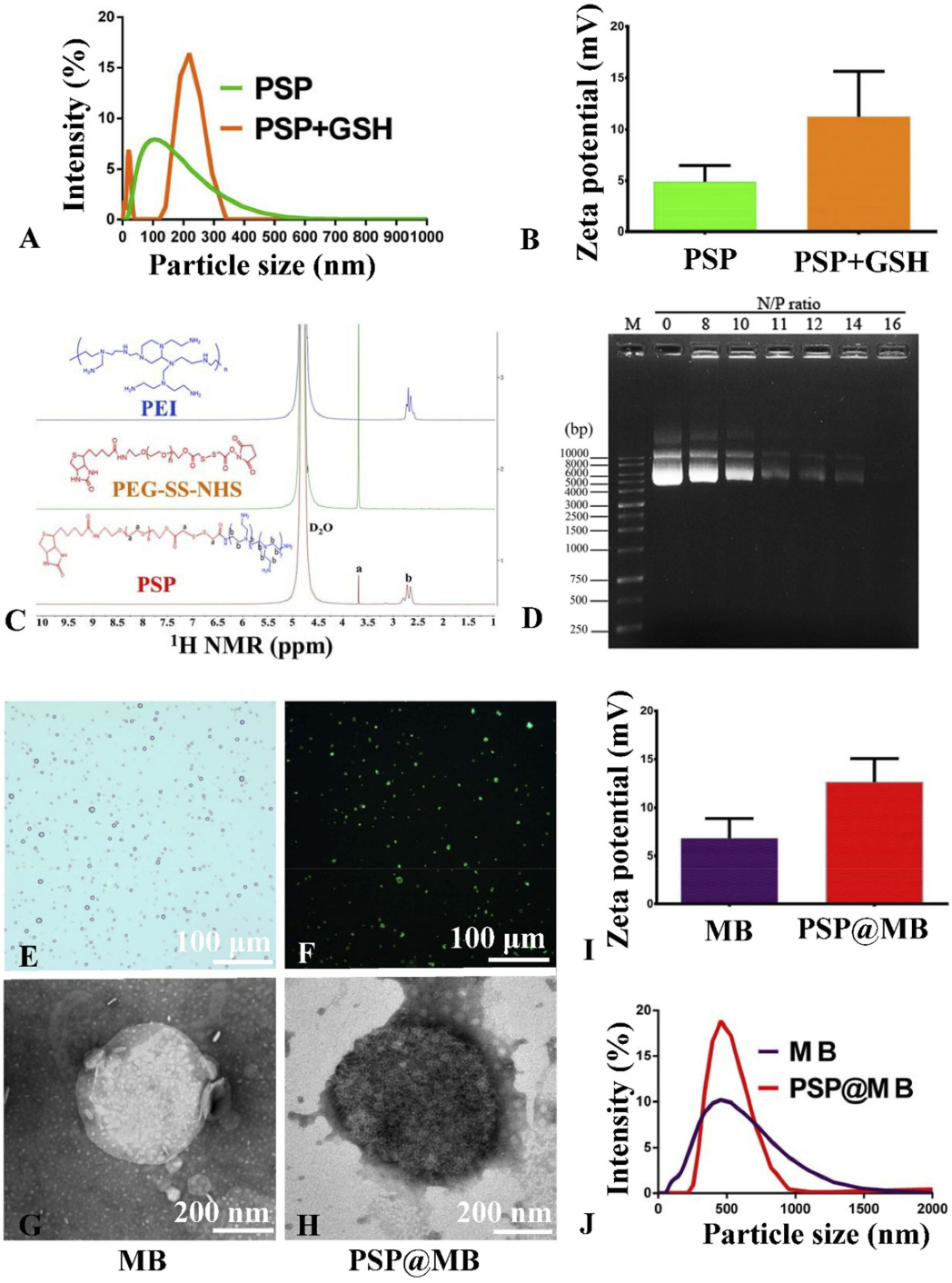

Figure 2 Characterization of the PSP, MB and PSP@MB.

Notes: (**A**) The dynamic light scattering (DLS) measurement indicated that the average diameters of the PSP NPs were approximately 100 nm and (**B**) showed a slight positive zeta potential of 4±2.5 mV due to the PEGylation. To evaluate the reduction sensitivity, the PSP NPs were incubated with 10 mM GSH for 2 h. (**A**) After the GSH treatment, the PSP NPs increased in size from 100±53 nm to 210±101 nm and (**B**) showed a change in the surface charge from 4±2.5 mV to 12±4.3 mV. (**C**) The successful synthesis of PSP confirmed by 1H NMR spectra of PSP in D_2O. The signals of PEG (3.65 ppm) in "a" and PEI (2.3–2.7 ppm) in "b" were found in the 1H NMR spectra of PSP. (**D**) To confirm the pDNA binding ability of PSP NPs, we checked the retardation of pDNA mobility in agarose-gel electrophoresis. The pDNA condensation ability of PSP NPs were tested with various N/P ratios (0, 8, 10, 11, 12, 14, 16). PSP showed beneficial complexation of pDNA. The pDNA were completely retarded at an N:P ratio of 16, which indicated that the PSP can complex the pDNA entirely. However, the optimized proportion for gene transfection between PSP@MB and pDNA complex is not just the N/P ratio of PSP/pDNA, but more important is the concentration of PSP@MB. (**E**) Microscope image of PSP@MB was showed. (**F**) FITC-streptavidin was conjugated with PSP NPs and MBs. Fluorescence microscope confirmed successful connection of PSP loaded MBs. (**J**) The DLS measurement showed that the average diameters of the MBs and PSP@MB were approximately 495±132 nm and 502±75 nm, and (**I**) zeta potential were 7±3.6 mV and 13±4.4 mV. Transmission electron microscope (TEM) images of MB (**G**) and PSP@MB (**H**) showed the similar particle size with DLS.

Abbreviations: PSP, polyethyleneglycol-SS-polyethylenimine; PSP@MB, polyethyleneglycol-SS-polyethylenimine@ microbubble; ^{1}H NMR, ^{1}H nuclear magnetic resonance; TEM, transmission electron microscope.

analysis revealed that the shapes of spheroids were the same as ALDH1$^+$ OCSC spheroids (Figure S2B). In the third week, the spheroids were collected and sorted with ALDEFLUOR^{TM} assay and flow cytometry analysis. The ALDH1$^+$ and ALDH1$^-$ cells were sorted by flow cytometry analysis. The percentage of ALDH1$^+$ cells were 54% (Figure S2B right) compared with A2780 monolayer cultures. After sorting, the ALDH1$^+$ cells and ALDH1$^-$ cells were cultured in a serum-free culture. The formation of ALDH1$^+$ OCSC spheroids were shown at one month (Figure S2C left). Of interest was the transition back from spheroid-to-monolayer when the ALDH1$^+$ OCSC spheroids were cultured with serum in a culture medium for three days (Figure S2C right).

Cytotoxicity Of PSP@MB

The cytotoxicity of the PSP@MB polyplexes was evaluated with CCK-8 assays. OCSCs and vascular endothelial cells (VECs) were co-incubated with PSP@MB for 24 h. A CCK-8 assay was applied to evaluate cell viability. The concentration of PSP@MB was 1.0–3.0 × 10^{10} MBs/mL. As shown in Figure 3A, after 24 h incubation with PSP@MB, the cell viability of OCSCs and VECs was >85% in each group, which suggested good biocompatibility of the PSP@MB.

SEM And CLSM Images Of OCSCs Intracellular Uptake Of PSP@MB Under Ultrasound

There are different cell uptake mechanisms at different acoustic pressures: at low acoustic pressures endocytosis is enhanced, while higher acoustic pressures favored uptake via membrane pores. The new mechanism of "sonoprinting" was mentioned in the process of real-time swept field confocal microscopy imaging.[14] In this article, the SEM imaging demonstrated the micropore in the membrane of OCSCs after exposure to different intensities of ultrasound combined with PSP@MB (scale bar=5 μm). At the OCSC membranes ultrasound generated reparable small pores (the yellow arrow), by which OCSCs could uptake plasmid DNA of extracellular fluids. More small pores would be generated under high ultrasound acoustic intensities (1.2 W/cm^2) than low ultrasound acoustic intensities (0.4 W/cm^2) (Figure 3B).

Ultrasound assisted the endocytosis and sonoporation of OCSCs. The optimal combined ultrasound parameters were (0.8 W/cm^2, 1 MHz, 20% duty cycle, 1 min). OCSCs were transfected with PSP@MB combined ultrasound for 10 min, 60 min, 3 h and 24 h. CLSM images of Cy5-labeled pDNA (red) loaded with PSP@MB and cell nuclei (blue) showed that in 60 mins there were more pDNA uptake of OCSCs in the PSP@MB group. And there were more pDNA into OCSCs in the PSP@MB+US group than another groups (Figure 3C).

Effect Of Ultrasound On The Transfection Efficiency Of PSP@MB/pDNA Into OCSCs

The combination of PSP@MB with ultrasound enhances the delivery of plasmids encoding EGFP reporter genes into OCSCs. Fluorescent images of OCSCs exposed to plasmid-containing different reagents, with or without ultrasound irradiation, respectively, after 24 h (Figure 4A). There were six groups: (a) Control (plasmid), (b) PSP, (c) MB +US, (d) Lipofectamine 2000, (e) Lipofectamine 3000, (f) PSP@MB+US. The optimized ultrasound parameters (0.8 W/cm^2, 1 MHz, 20% duty cycle, 30 s), (scale bar=100 μm). Transfection efficiency rate was evaluated by flow cytometry (Figure 4B). Transfection efficiency rate was represented as histograms. The transfection efficiency rate was 15.8% in the PSP@MB and ultrasound group, higher than Lipofectamine 3000 group (12.1%) or MB and US group (5.6%) (Figure 4C). Data are represented as mean ± standard deviation; n = 3; $^{**}P<0.01$.

Effect Of Ultrasound On The Transfection Efficiency Of PSP@MB/pDNA Into A2780

The combination of PSP@MB with ultrasound enhances the delivery of plasmids encoding EGFP reporter genes into A2780. Fluorescent images of A2780 exposed to plasmid-containing different reagents, with or without ultrasound irradiation, respectively, after 24 h (Figure S3A). There were six groups: (a) Control (plasmid), (b) PSP, (c) MB +US, (d) Lipofectamine 2000, (e) Lipofectamine 3000, (f) PSP@MB+US. The optimized ultrasound parameters (0.8 W/cm^2, 1 MHz, 20% duty cycle, 30 s), (scale bar=100 μm). Transfection efficiency rate was evaluated by flow cytometry (Figure S3B). Transfection efficiency rate was represented as histograms. The transfection efficiency rate was 31.4% in the PSP@MB and ultrasound group, lower than Lipofectamine 2000 group (37%), but higher than Lipofectamine 3000 group (25%) or MB+US group

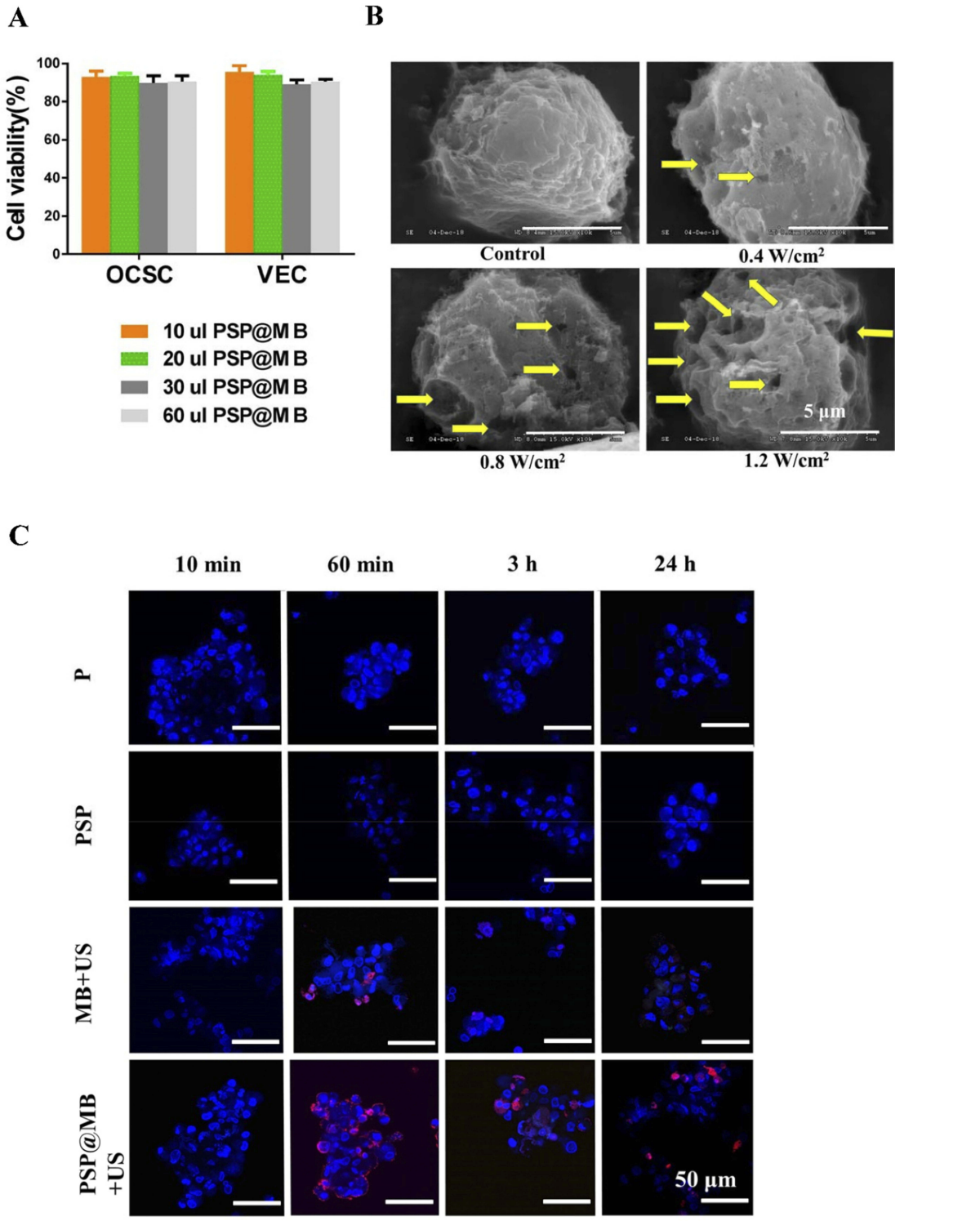

Figure 3 Cell viability, SEM and CLSM images of OCSCs.

Note: (**A**) The OCSCs and vascular endothelial cells (VECs) were incubated with the concentration of PSP@MB (1.0–3.0×10^{10} MBs/mL) for 24 h, respectively. CCK-8 assay was showed that the cell viability of OCSCs and VECs was >85% in each group, which suggested good biocompatibility of the PSP@MB in vitro. (**B**) The SEM images of OCSCs under different acoustic intensity and PSP@MB (scale bar =5 μm). Ultrasound generated reparable small pores (the yellow arrow) at the surface of OCSC membranes, by which could enhance OCSC uptake of plasmid DNA. More small pores would be generated under high acoustic intensity (1.2 W/cm^2) compared to low acoustic intensity (0.4 W/cm^2). (**C**) CLSM images of OCSCs transfected with PSP@MB combined ultrasound for 10 min, 60 min, 3 h and 24 h. There was more pDNA into OCSC in the PSP@MB+US group compared to MB+US group or PSP group. It showed that PSP@MB combined ultrasound could efficiently deliver pDNA to OCSC with sonoporation. pDNA was labeled with Cy5 (red) and cell nuclei were stained by DAPI (blue).

Abbreviations: VEC, vascular endothelial cell; pDNA, plasmid DNA; min, minute; h, hour; SEM, scanning electron microscope.

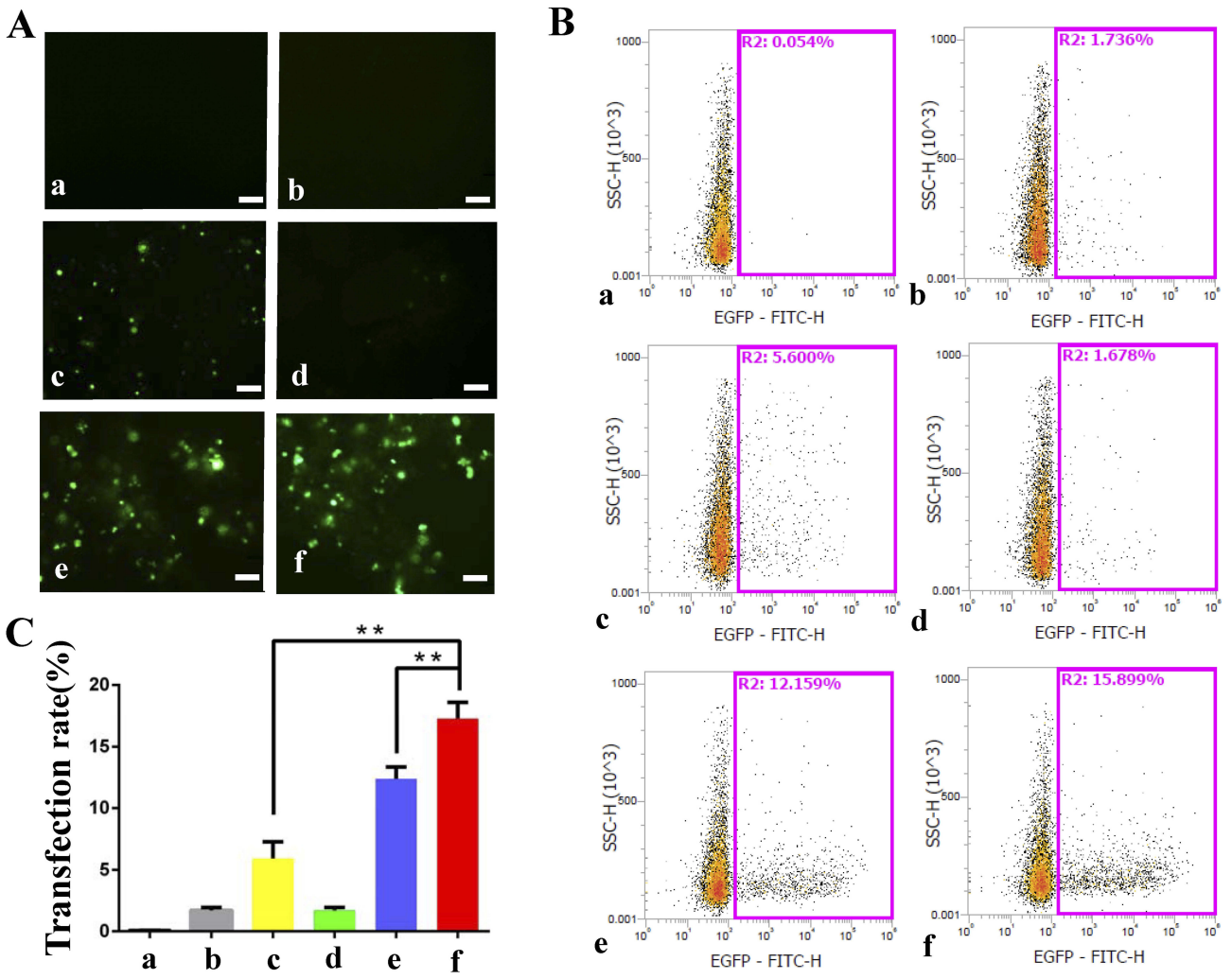

Figure 4 Effect of ultrasound on the transfection efficiency of PSP@MB/pDNA into OCSC.
Notes: (**A**) Fluorescent images of OCSC exposed to plasmid-containing different reagents: PSP, MB, Lipofectamine 2000, Lipofectamine 3000, PSP@MB, with or without ultrasound irradiation, respectively, after 24 h. There were six groups: (a) Control (pDNA), (b) PSP, (c) MB+US, (d) Lipofectamine 2000, (e) Lipofectamine 3000, (f) PSP@MB +US. The optimized ultrasound parameters (0.8 W/cm^2, 1 MHz, 20% duty cycle, 30 s), (scale bar=100 μm). (**B**) Transfection efficiency rate was evaluated by flow cytometry. (**C**) Transfection efficiency rate was represented as histograms. The transfection efficiency rate was 15.8% in the PSP@MB + ultrasound group, higher than Lipofectamine 3000 group (12.1%) or MB + US group (5.6%). Data are represented as mean ± standard deviation; n = 3; $^{**}P < 0.01$.
Abbreviations: PSP, PEG-SS-PEI; PSP@MB, PEG-SS-PEI@microbubble; US, ultrasound.

(11%). (Figure S3C). Data are represented as mean ± standard deviation; n = 3; $^{**}P<0.01$.

Contrast-Enhanced Ultrasound Imaging Of Xenograft Of Nude Mice In Vivo

Contrast-enhanced ultrasound (CEUS) and B mode imaging sequences were recorded in the OCSC-bearing xenograft mice model. PSP@MB (Figure 5A) and MB (Figure 5B) were injected from tail vein after deep anesthesia, respectively. In vivo ultrasound imaging was performed using Aplio 500 ultrasound (Toshiba) with an 18 MHz probe (MS250) at different time points (before injection, 1 s, 30 s, 60 s, 120 s, 180 s). Line chart summarized the mean ± standard deviation of mean intensity of CEUS, showing that the PSP@MB was a fantastic ultrasound contrast agent (Figure 5C).

LIFU Combined With PSP@MB On In Vivo Gene Transfection Efficiency

In vivo bioluminescence imaging showed the expression of plasmids encoding luciferase reporter gene in subcutaneous xenografts of nude mice on 48 h after tail vein injection (Figure 6A). The five groups were (a) US, (b) PSP, (c) US+MB, (d) Lipofectamine 3000, (e) US +PSP@MB. The LIFU parameters were: (1 MHz, 10,000 cycles, voltage 250 mV, exposure time 5 min). The region

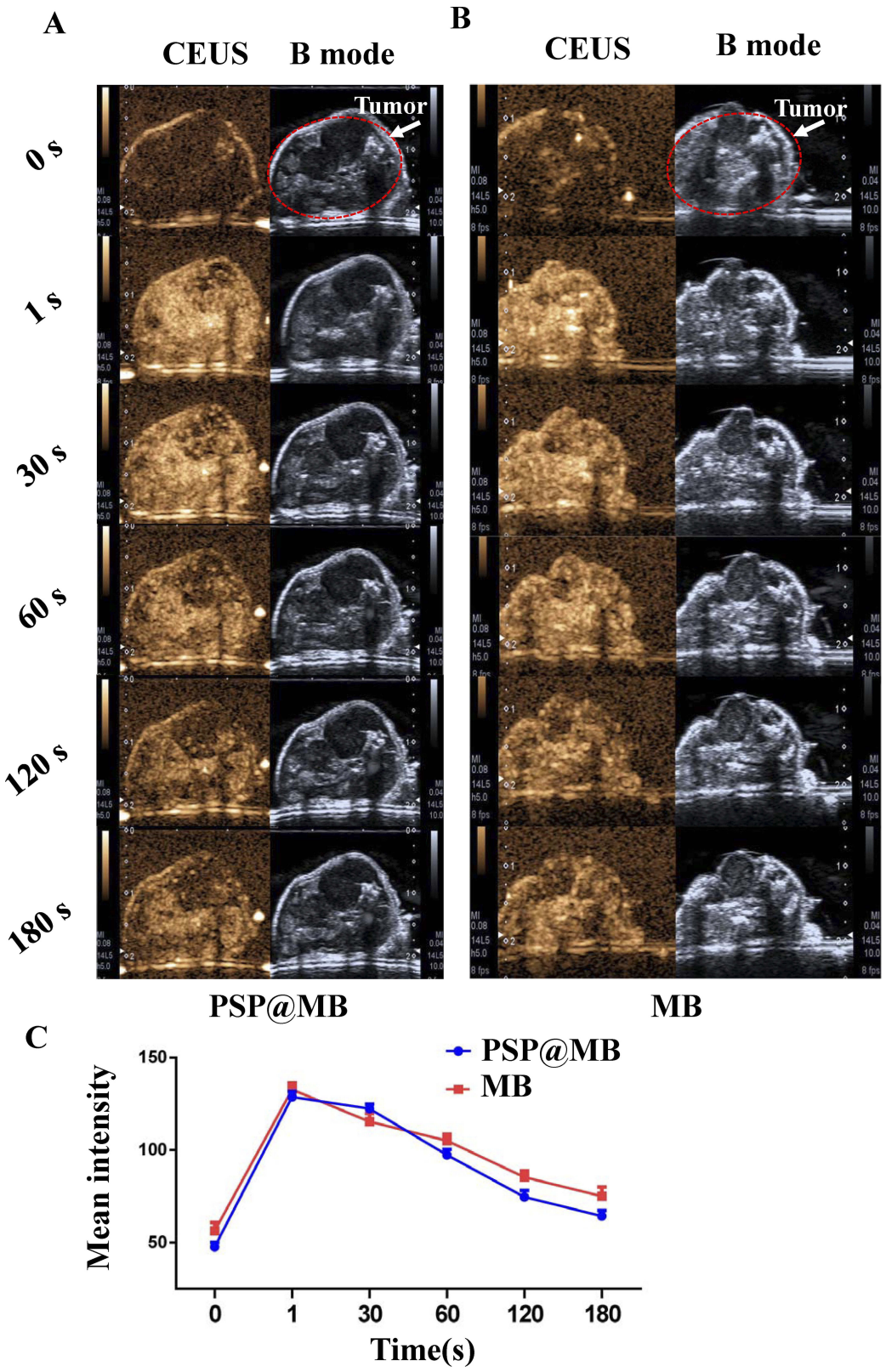

Figure 5 Contrast-enhanced ultrasound imaging of xenograft of nude mice in vivo.

Notes: Segmented multi-slice contrast-enhanced ultrasound (CEUS) and B mode imaging sequences were recorded in the OCSC-bearing xenograft mice model. PSP@MB (**A**) or MB (**B**) were injected from tail vein after deep anesthesia, respectively. In vivo ultrasound imaging was performed using Aplio 500 ultrasound (Toshiba) with an 18 MHz probe (MS250) at different time points (before injection, 1 s, 30 s, 60 s, 120 s, 180 s). (**C**) Line chart summarized the mean ± standard deviation of mean intensity of CEUS, showing that the PSP@MB was a fantastic ultrasound contrast agent.

Abbreviations: s, second; CEUS, contrast-enhanced ultrasound.

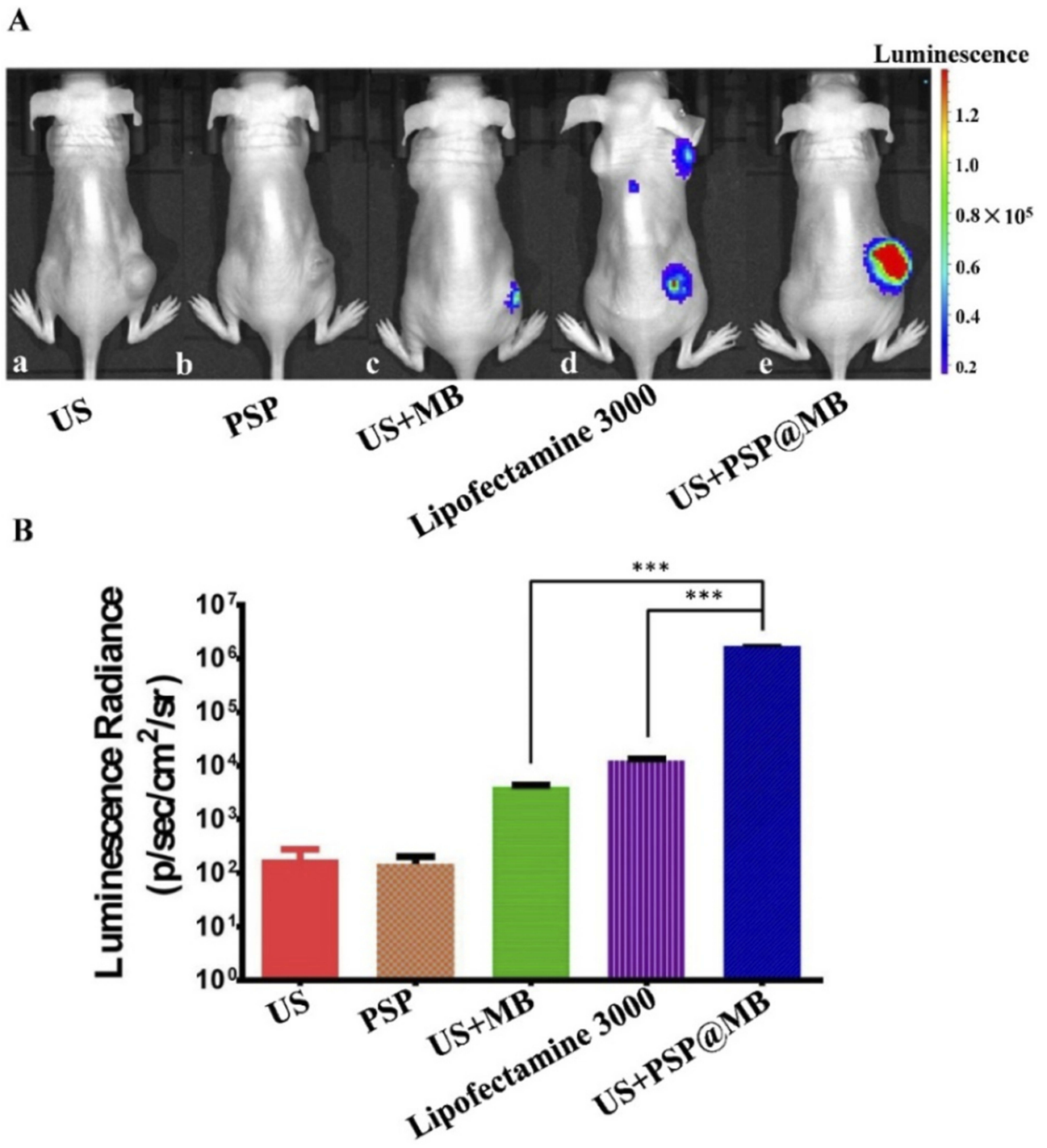

Figure 6 LIFU and PSP@MB deliver luciferase reporter gene expression in a tumor xenograft model.
Notes: (**A**) In vivo bioluminescence imaging showed the expression of plasmids encoding luciferase reporter gene in subcutaneous xenografts of nude mice on 48 h after tail vein injection. The five groups were (a) US, (b) PSP, (c) US+MB, (d) Lipofectamine 3000, (e) US+PSP@MB. The LIFU parameters were: (1 MHz, 10,000 cycles, voltage 250 mV, exposure time 5 min). The region of interest (ROI) was selected in subcutaneous xenografts of nude mice with the same color bar. (**B**) The luminescence radiance of ROI was represented as histograms. It showed that there was higher transfection in the US+PSP@MB group compared to the US+MB group and lipofectamine 3000 group. Data are represented as mean ± standard deviation; n = 3; ***P<0.001.
Abbreviation: ROI, region of interest.

of interest (ROI) was selected in subcutaneous xenografts of nude mice with the same color bar. The ROI data showed that there was higher transfection in the US +PSP@MB group compared to the US+MB group and lipofectamine 3000 group (Figure 6B). Data are represented as mean ± standard deviation; n = 3; ***P<0.001.

Biosafety Evaluation

To evaluate the biocompatibility of PSP@MB, histological examination of hematoxylin and eosin (H&E) staining of vital organ (heart, liver, spleen, lung, kidney) sections were detected. The result of H&E staining assay showed symptoms of swell, fatty and vacuolar in the liver cells treated by lipofectamine 3000 (yellow arrow). The PSP@MB+US group (blue arrow points) demonstrated the normal morphology of liver cells compared with plasmid group (Figure 7A). Two pathologists confirmed the histopathological diagnosis of diffuse hepatic edema in lipofectamine 3000 group. The histopathological results demonstrated PSP@MB had excellent biocompatibility, but lipofectamine 3000 had abnormal liver damage in at a certain concentration in vivo.

To evaluate the biocompatibility of PSP@MB, whole blood and blood serums were collected at 48 h after intravenous injection of PSP@MB or lipofectamine 3000. The liver functions (ALT and AST), renal functions (Crea, Urea and UA), Direct Bilirubin (D BILI) and routine blood parameters (hemoglobin and white blood cell) were tested. All the biochemical parameters in serum and routine blood tests remained at a normal range in PSP@MB and ultrasound group. The normal direct bilirubin indicated that there was no hemolysis, showing the good hemocompatibility of PSP@MB. Compared with PSP@MB, the lipofectamine 3000 group reported elevated liver functions (ALT and AST) and D BILI, but normal renal function (Crea) and routine blood parameters (hemoglobin and white blood cell), which showed that lipofectamine 3000 resulted in some liver function lesions in vivo (Figure 7B). The results exhibited that PSP@MB outbalanced lipofectamine 3000 in biocompatibility at a certain concentration in vivo.

Discussion

Ovarian cancer is known to have the highest mortality rate among malignant gynecological diseases.[2] Cancer stem cells (CSCs) are at the top of the hierarchy in multiple cancer types and are at the root of tumor recurrence and chemo-resistance.[21,22] Killing CSCs is thought to be a key part of effective antitumor therapies.[21] Gene therapy has been considered to be a promising therapy for CSCs and cancer cells.[23–25] However, gene delivery still faces many limitations due to their negative charge, high molecular weight, instability in biological environments and low levels of transfection. To overcome these drawbacks, therapeutic genes should be carried in a stable nanocarrier and released at specific target site.[26] There are two kinds of vectors for gene delivery: viral and non-viral vectors.

With the development of material technology, non-viral vectors are intensively explored to deliver therapeutic genes in vitro or in vivo due to their great versatility. As compared to viral vectors, non-viral vectors possess advantages of low immunogenicity and cytotoxicity, easy modification with targeting ligands and powerful gene-loading capacity without size limitations.[8] Non-viral vectors consist of polymers, liposomes, peptides, carbon nanotubes, gold nanoparticles and magnetic nanoparticles.[26]

Many strategies have been proposed to obtain effective gene delivery to target cells. An effective gene delivery system should have the following properties: (i) be able to carry and protect the therapeutic genes; (ii) accumulate at targeted tissues, and (iii) release the entrapped payload at the targeted tissue. Non-viral vectors are usually taken up by the cells through the endosomal pathway in vivo. Due to the low pH and digestive enzymes within endosomes, genes face the risk of degradation before reaching their site of action.[26]

There are two kinds of stimuli-responsive gene release systems; endogenous stimuli-responsive systems (such as pH-, redox reaction-, enzymatic-triggered approaches) and exogenous triggered gene release strategies (such as ultrasound, light, heat, magnetic field). However, triggered gene release by intrinsic physical and biological factors faces many limitations. The environment of the disease site is heterogeneous and strongly dependent on the patient's condition such as illness or diet; therefore, the effects are not easy to predict. Compared to endogenous triggers, exogenous triggered gene release is spatiotemporally controlled via the active management of external stimuli.[26]

25 kDa PEI is one of the most effective gene vectors characterized by a high positive charge density and the "proton sponge effect", by which genes can be robustly condensed and achieve evasion from endosomes or lysozymes. However, high gene transfection efficiency always comes hand in hand with high cytotoxicity due to the high positive charge density of 25 kDa PEI. To achieve effective and safe gene transfection, many groups have applied modifications to PEI.[9,10] PEGylation shielded the positive surface charges of PEI with disulfide bonds, leading to decreased cytotoxicity, improved stability and prolonged circulation. PEGylation would rapidly disappear due to GSH as soon as arriving at the tumor sites. This is because the level of GSH in cancer cells is 100-fold higher than the normal ranges. GSH causes the disulfide bond to fracture

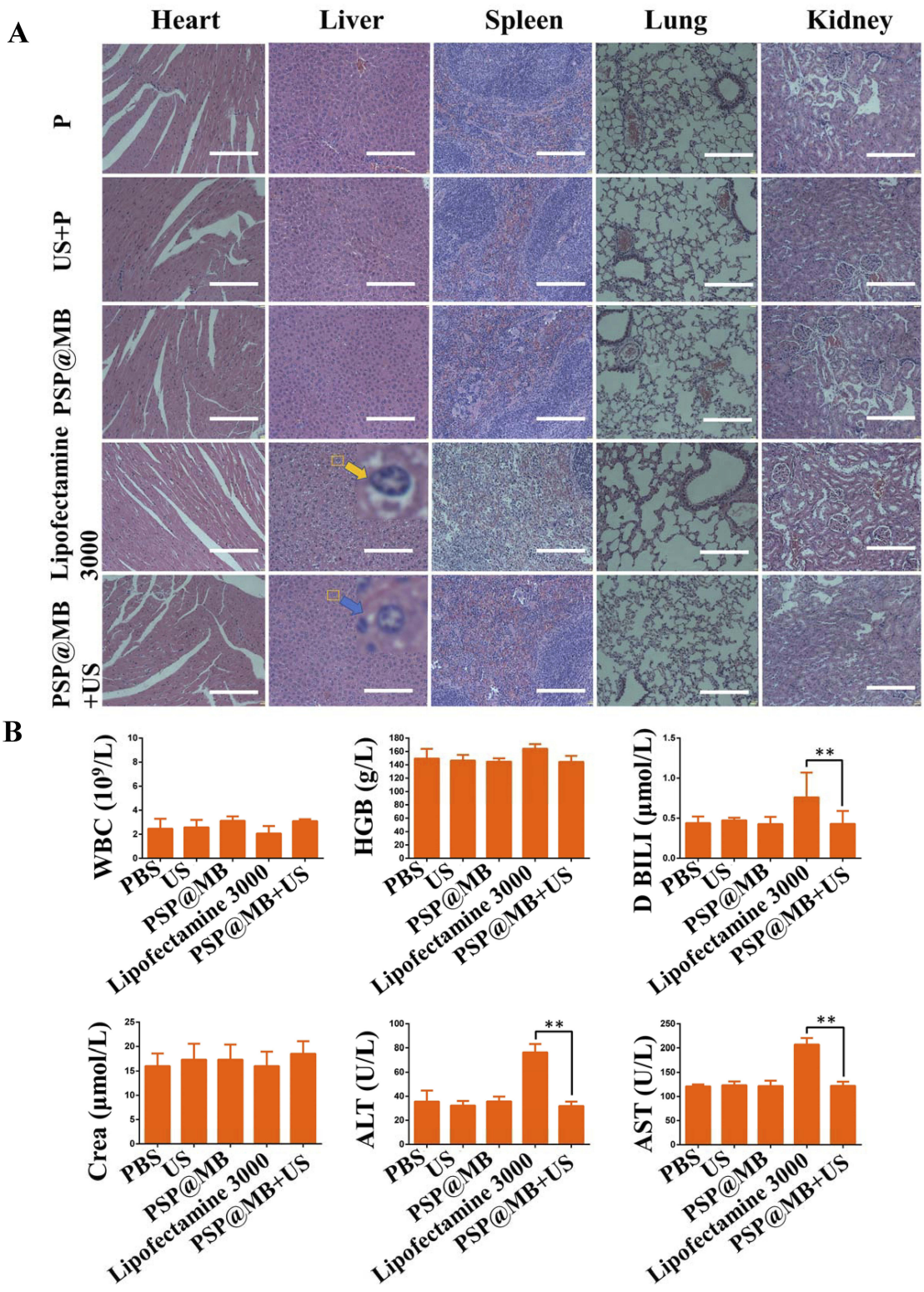

Figure 7 Biosafety evaluation.

Notes: (**A**) Histological examination of hematoxylin and eosin (H&E) staining of vital organ (heart, liver, spleen, lung, kidney) sections. The result of H&E staining assay showed symptoms of swell, fatty and vacuolar in the liver cells treated by lipofectamine 3000 (yellow arrow). The PSP@MB+US group (blue arrow) demonstrated the normal morphology of liver cells compared with plasmid group (scale bar=100 μm). (**B**) The liver functions (ALT and AST), the renal functions (Crea), Direct Bilirubin (D BILI) and routine blood parameters (hemoglobin and white blood cell) were tested. All the biochemical parameters in serum and routine blood test remained at a normal range in PSP@MB and ultrasound group. Compared with PSP@MB and ultrasound group, the activity of ALT, AST and D BILI were increased significantly in lipofectamine 3000 group. The histopathological and liver functions results exhibited that PSP@MB displayed better biocompatibility than lipofectamine 3000 at a certain concentration in vivo. Data are represented as mean ± standard deviation; n = 3; $^{**}P<0.01$.

and can be used as a trigger for redox stimulus gene release. Finally, PEI could facilitate escape from endosomes and release the pDNA intracellularly.[27] It had been reported that PSP nanoparticles were used as a promising gene vector in glioblastoma[10] and gastric cancer.[9] Xiu et al reported that the PEG/PEI/DNA nanoparticles at a mass ratio of 10:2.5:1 with the gel retardation assay showed the optimum gene compression.[28]

To obtain higher gene transfection, the biotinylated PSP nanoparticles were connected to avidinylated MBs via the avidin-biotin method. As theranostic particles, PSP@MBs possess a dual ability for imaging as well as treatment to facilitate the detection and treatment of ovarian cancer. The lipid MB components have excellent echo signals for ultrasound imaging and optical coherence tomography imaging, while the PSP serves as a high loading vector of therapeutic materials.[29] To achieve more efficient gene transfection, besides modifying the gene vector, different parameters of the ultrasound, such as intensity, duty cycle, irradiation time, and PSP@MB concentration were modified as well. The PSP@MB complexes showed the beneficial capacity of loading the pDNA extracellularly and releasing the loaded pDNA intracellularly into the cytoplasm to enter the nucleus.[30]

Ultrasound-mediated gene delivery is a promising non-viral method for the treatment of cancer cells.[31–33] LIFU has certain special advantages such as being non-invasive, having deep tissue penetration and the ability to focus on tumor tissues. LIFU has been safely and locally implemented to raise the delivery potency of drugs or genes into cancer cells. The use of gas-filled MBs as ultrasound contrast agents in the bloodstream generates resonant volumetric oscillations in response to rapid variations in acoustic pressure, which lowers the acoustic energy needed for these processes. In an ultrasonic field, MBs would oscillate and lead to a stable cavitation. Such stable oscillations create a liquid flow around the MBs, known as "microstreaming". When these oscillating MBs were in close vicinity of cells, these cells would experience shear stress. Consequently, elevated levels of shear stress induced by ultrasound can enhance the cellular uptake of macromolecular plasmids. Therefore, the UTMD technique, which has been conventionally used in clinical diagnostic imaging, holds considerable promise as an effective strategy to achieve the targeted delivery of genes from nanoparticle formulations to the cancer cell. Previous studies have demonstrated that the gene transfection efficiency was modest using ultrasound-mediated gene delivery with neutral MBs.[29,34] In spite of this, UTMD has many advantages, such as non-invasiveness, repeatability and targeted gene delivery into some localized tissues.[29,35] Previous studies showed that the combination of UTMD with cationic liposomes could enhance gene transfection. Our previous experiments demonstrated that the combination of UTMD with PEI can improve gene transfection of cancer cells with optimized parameters in vitro and in vivo. Another study showed that ultrasound and PEI can specifically increase gene transfection, the mechanism being that ultrasound increases endocytosis due to an increase in the intracellular calcium levels.[36]

To investigate the gene transfection efficiency of OCSCs with ultrasound and PSP@MB, gene transfection was performed on OCSCs and the EGFP pDNA was used as the reporter gene. The 48 h transfection efficiencies of PSP@MB and ultrasound showed that the optimal concentration ratio and ultrasound parameters can enhance the gene transfection efficiency of OCSCs. Ultrasound-mediated nanoparticle delivery with MBs retained a high efficiency of targeted gene delivery as a spatial and temporal tool. Sonoporation, which resulted from ultrasound and MB cavitation, was found to overcome the limitations of PEGylated PEI.

This study demonstrates that PSP@MB and LIFU enabled the significant promotion of in vitro and in vivo expression of pDNA to OCSCs and xenograft tumors. This PSP@MB and LIFU gene delivery system possessed the following favorable properties: (i) Non-invasiveness and high tissue-penetrating ability, where this feature of LIFU could offer effective gene delivery for spatiotemporal control. LIFU could also improve extravasation from the vasculature and penetration through the extracellular matrix to the tumor and promote the efficacy of gene delivery. (ii) PEGylation shielded the positive surface charges of PEI with disulfide bonds, leading to decreased cytotoxicity, improved stability and prolonged circulation. (iii) PEGylation shielding would rapidly disappear due to GSH as soon as arriving at the tumor. (iv) Sonoporation, enhanced endocytosis and sonoprinting generated by LIFU and MBs would promote the entry of PSP/plasmid into cancer cells. (v) In the cytoplasm, plasmids can be protected from endosome or lysozyme capture due to the "proton sponge effect" by the PEI.

To evaluate whether ultrasound and PSP@MBs could promote gene uptake into OCSCs, the gene was labeled with Cy5 and incubated with OCSCs. Cell uptake efficiency was measured by confocal laser scanning microscopy. The results are shown in Figure 3C. Compared to

all other groups, the uptake efficiency of PSP@MB and ultrasound group displayed much stronger red fluorescence. This was attributed to the generation of sonoporation by ultrasound and MBs. In this study, scanning electron microscopy (SEM) was used to investigate the ultra-structural modifications of cell membranes induced by sonoporation (Figure 3B). The study showed that sonoporation in the presence of PSP@MB and ultrasound induced the formation of a significant number of permeant structures at the membrane level. The number and the size of these transient pores in the cell membrane were positively correlated with the enhanced intracellular uptake of DNA. De Cook et al showed that there were three major mechanisms concerning the delivery of nanoparticles to the cells using ultrasound and nanoparticle-loaded MBs: sonoporation, enhanced endocytosis and sonoprinting. Additionally, the acoustic pressure strongly influences which uptake mechanism occurs: at low acoustic pressures endocytosis is enhanced, while higher acoustic pressures favor uptake via membrane pores. Sonoprinting is the process where nanoparticles were directly deposited onto the cell membrane in patches by the nanoparticle-loaded MBs.[37]

To evaluate whether ultrasound and PSP@MB enhanced gene delivery into tumor tissue in vitro and in vivo, EGFP reporter genes or luciferase reporter genes were delivered to A2780 and OCSCs in vitro and to subcutaneous xenografts in vivo via the combination of ultrasound with PSP@MB. As shown in Figure 4B, the gene transfection rate of PSP@MB and ultrasound group was 15 times greater than that of the PSP group. In addition, the transfection rate of PSP@MB and ultrasound group was triple than that of the MB and ultrasound group. The tumor targeting capability of PSP@MB complexes was assessed in vivo following systemic administration. We examined the accumulation of luciferase reporter gene in the tumor after intravenous injection of PSP@MB and LIFU exposure by the IVIS Lumina HTX. PSP@MB and LIFU showed a significantly stronger fluorescence signal in the tumor region at 48 h compared to MB and LIFU group and lipofectamine 3000 group, further confirming a more effective tumor targeting effect of PSP@MB and LIFU (Figure 6A). In the tumor tissue, the sonoporation generated by UTMD heightened the permeation and uptake of PSP/pDNA complexes into tumor tissues. Subsequently, when the PSP nanoparticles reached the tumor tissues, the disulfide bonds of PSP was cleaved in the presence of high concentrations of GSH. The de-PEGylated PEI/pDNA nanoparticles can achieve endosomal escape and release the pDNA into the cytoplasm in a spatiotemporally controlled manner. Compared to the PSP@MB and LIFU group, the lipofectamine 3000 group had some non-specific background signal in the non-tumor area (Figure 6A). As a cationic carrier, lipofectamine 3000 is easily phagocytized by the mononuclear phagocyte system (eg, liver, spleen and lung) in the blood circulation. However, surface modification of PSP@MB with PEG reduces the non-specific uptake by Kupffer cells in the liver, also, the passive targeting effect of LIFU to the tumor area increased the enhanced permeability and retention effect (EPR) effects, which is why the PSP@MB and ultrasound group possess specific signals in the tumor area in vivo. Compared to the PSP@MB and US group, the lipofectamine 3000 group had a two-fold increase in the liver functions (ALT, AST and D BILI), which showed that the use of lipofectamine 3000 resulted in abnormal liver function in vivo. However, the PSP@MB and LIFU group reported normal data compared to the plasmid group (Figure 7B). These results proved the good biocompatibility of the PSP@MB and ultrasound delivery system.

Conclusion

In this article, we synthesized and characterized an ultrasound-triggered and GSH-sensitive gene delivery system, PSP@MB for targeting cancer stem cells. The combination of ultrasound with PSP@MB/pDNA not only showed low cytotoxicity and remarkable cellular uptake in vitro, but also demonstrated successful targeting to the tumor tissue and no obvious tissue toxicity in vivo. PSP@MB exhibited the capability to enhance ultrasound contrast for the detection and treatment of cancer. In summary, the combination of ultrasound with the gene vector PSP@MB, with optimal parameters, could achieve the effective delivery of pDNA with low cytotoxicity in vitro and in vivo. This study presents an efficient, safe, low-toxic, non-viral gene transfection strategy based on the combination of ultrasound and PSP@MB besides showing potential for gene therapy of ovarian cancer.

Acknowledgements

This work is supported by the Research Projects of National Natural Science Foundation of China (No. 81671707, 81527803, 81420108018, 81971621), National Key R&D Program of China (No.2018YFC0115900), the Young Scientists Fund of the National Natural Science Foundation of China (81901764), the Natural Science Foundation of

Guangdong Province (No. 2018A030313678), the Natural Science Foundation of Guangdong Province (No. 2016A030311054), the Zhejiang Science and Technology Project (No. 2019C03077), the Research Projects of Guangzhou Technology Bureau (No. 201607010201), the PhD Research Startup Foundation of the Third Affiliated Hospital of Guangzhou Medical University (No. 2018B04), the Research Fund for Lin He's Academician Workstation of New Medicine and Clinical Translation, the Shenzhen Health and Family Planning System Scientific Research Project (No. 201607040), the 2018 Youth Scientific Research Project of the Third Affiliated Hospital of Guangzhou Medical University (No. 2018Q28, No. 2018Q03), and the Medical Science and Technology Research Fund Project of Guangdong Province (No. B2019136). Scientific and Technological Livelihood Projects of Liwan district (No. 201904003).

Disclosure

The authors report no conflicts of interest in this work.

References

1. Huang X, Borgstrm B, Stegmayr J, et al. The molecular basis for inhibition of stemlike cancer cells by salinomycin. *ACS Cent Sci*. 2018;4(6):760–767. doi:10.1021/acscentsci.8b00257
2. Siegel RL, Miller KD, Jemal A. Cancer statistics, 2018. *CA Cancer J Clin*. 2018;68:7–30. doi:10.3322/caac.21442
3. House CD, Jordan E, Hernandez L, et al. NFκB promotes ovarian tumorigenesis via classical pathways that support proliferative cancer cells and alternative pathways that support ALDH+ cancer stem-like cells. *Cancer Res*. 2017;77:6927–6940. doi:10.1158/0008-5472.CAN-17-0366
4. Li J, Condello S, Thomes-Pepin J, et al. Lipid desaturation is a metabolic marker and therapeutic target of ovarian cancer stem cells. *Cell Stem Cell*. 2017;20:303–314.e5. doi:10.1016/j.stem.2016.11.004
5. Seo EJ, Kwon YW, Jang IH, et al. Autotaxin regulates maintenance of ovarian cancer stem cells through lysophosphatidic acid-mediated autocrine mechanism. *Stem Cells*. 2016;34:551–564. doi:10.1002/stem.2279
6. Vaidyanathan S, Orr BG, Banaszak Holl MM. Role of cell membrane-vector interactions in successful gene delivery. *Acc Chem Res*. 2016;49(8):1486–1493. doi:10.1021/acs.accounts.6b00200
7. Guan X, Guo Z, Lin L, et al. Ultrasensitive pH triggered charge/size dual-rebound gene delivery system. *Nano Lett*. 2016;16(11):6823–6831. doi:10.1021/acs.nanolett.6b02536
8. Zhang H, Chen Z, Du M, et al. Enhanced gene transfection efficiency by low-dose 25 kDa polyethylenimine by the assistance of 1.8 kDa polyethylenimine. *Drug Deliv*. 2018;25(1):1740–1745. doi:10.1080/10717544.2018.1510065
9. Luo X, Peng X, Hou J, et al. Folic acid-functionalized polyethylenimine superparamagnetic iron oxide nanoparticles as theranostic agents for magnetic resonance imaging and PD-L1 siRNA delivery for gastric cancer. *Int J Nanomedicine*. 2017;12:5331–5343. doi:10.2147/IJN
10. Lei Y, Wang J, Xie C, et al. Glutathione-sensitive RGD-poly(ethylene glycol)-SS-polyethylenimine for intracranial glioblastoma targeted gene delivery. *J Gene Med*. 2013;15(8–9):291–305. doi:10.1002/jgm.2726
11. Wang S, Zhou Z, Wang Z, et al. Gadolinium metallofullerene-based activatable contrast agent for tumor signal amplification and monitoring of drug release. *Small*. 2019;15(16):e1900691. doi:10.1002/smll.v15.16
12. Wang S, Wang Z, Yu G, et al. Tumor-specific drug release and reactive oxygen species generation for cancer chemo/chemodynamic combination therapy. *Adv Sci (Weinh)*. 2019;6(5):1801986. doi:10.1002/advs.201801986
13. Eggen S, Fagerland SM, Mørch Ý, et al. Ultrasound-enhanced drug delivery in prostate cancer xenografts by nanoparticles stabilizing microbubbles. *J Control Release*. 2014;187:39–49. doi:10.1016/j.jconrel.2014.05.020
14. De Cock I, Lajoinie G, Versluis M, et al. Sonoprinting and the importance of microbubble loading for the ultrasound mediated cellular delivery of nanoparticles. *Biomaterials*. 2016;83:294–307. doi:10.1016/j.biomaterials.2016.01.022
15. Li Y, Lin Y, Liufu C, et al. Research of gene delivery mediated by ultrasound, microbubble and folate-modified chitosan nanoparticles. *Curr Mol Med*. 2018;18(6):383–391. doi:10.2174/1566524018666181109121509
16. Jain A, Cheng K. The principles and applications of avidin-based nanoparticles in drug delivery and diagnosis. *J Control Release*. 2017;245:27–40. doi:10.1016/j.jconrel.2016.11.016
17. Fan CH, Ting CY, Lin CY, et al. Noninvasive, targeted, and non-viral ultrasound-mediated GDNF-plasmid delivery for treatment of Parkinson's disease. *Sci Rep*. 2016;6:19579. doi:10.1038/srep19579
18. Luo W, Wen G, Yang L, et al. Dual-targeted and pH-sensitive doxorubicin prodrug-microbubble complex with ultrasound for tumor treatment. *Theranostics*;2017. 452–465. doi:10.7150/thno.16677
19. Ishiguro T, Sato A, Ohata H, et al. Establishment and characterization of an in vitro model of ovarian cancer stem-like cells with an enhanced proliferative capacity. *Cancer Res*. 2016;76:150–160. doi:10.1158/0008-5472.CAN-15-0361
20. Park YT, Jeong JY, Lee MJ, et al. MicroRNAs overexpressed in ovarian ALDH1-positive cells are associated with chemoresistance. *J Ovarian Res*. 2013;6:18. doi:10.1186/1757-2215-6-18
21. Nassar D, Blanpain C. Cancer stem cells: basic concepts and therapeutic implications. *Annu Rev Pathol*. 2016;11:47–76. doi:10.1146/annurev-pathol-012615-044438
22. Medema JP. Cancer stem cells: the challenges ahead. *Nat Cell Biol*. 2013;15:338–344. doi:10.1038/ncb2717
23. de Sousa E Melo F, Kurtova AV, Harnoss JM, et al. A distinct role for Lgr5(+) stem cells in primary and metastatic colon cancer. *Nature*. 2017;543:676–680. doi:10.1038/nature21713
24. Shimokawa M, Ohta Y, Nishikori S, et al. Visualization and targeting of LGR5(+) human colon cancer stem cells. *Nature*. 2017;545:187–192. doi:10.1038/nature22081
25. Yang C, Li B, Yu J, et al. Ultrasound microbubbles mediated miR-let-7b delivery into CD133+ ovarian cancer stem cells. *Biosci Rep*. 2018;38(5). doi:10.1042/BSR20180922
26. Do HD, Couillaud BM, Doan BT, et al. Advances on non-invasive physically triggered nucleic acid delivery from nanocarriers. *Adv Drug Deliv Rev*. 2019;138:3–17. doi:10.1016/j.addr.2018.10.006
27. Liu Y, Xu CF, Iqbal S, et al. Responsive nanocarriers as an emerging platform for cascaded delivery of nucleic acids to cancer. *Adv Drug Deliv Rev*. 2017;115:98–114. doi:10.1016/j.addr.2017.03.004
28. Guan X, Guo Z, Wang T, et al. A pH-responsive detachable PEG shielding strategy for gene delivery system in cancer therapy. *Biomacromolecules*. 2017;18:1342–1349. doi:10.1021/acs.biomac.7b00080
29. Yoon YI, Kwon YS, Cho HS, et al. Ultrasound-mediated gene and drug delivery using a microbubble-liposome particle system. *Theranostics*. 2014;4:1133–1144. doi:10.7150/thno.9945
30. Chang Kang H, Bae YH. Co-delivery of small interfering RNA and plasmid DNA using a polymeric vector incorporating endosomolytic oligomeric sulfonamide. *Biomaterials*. 2011;32:4914–4924. doi:10.1016/j.biomaterials.2011.03.042
31. Yang C, Li Y, Du M, Chen Z. Recent advances in ultrasound-triggered therapy. *J Drug Target*. 2018;27:1–18. doi:10.1080/1061186X.2018.1455841

32. Luo MH, Yeh CK, Situ B, Yu JS, Li BC, Chen ZY. Microbubbles: a novel strategy for chemotherapy. *Curr Pharm Des*. 2017;23(23):3383–3390. doi:10.2174/1381612823666170113092148
33. Yu J, Chen Z, Li Y, et al. Echogenic chitosan nanodroplets for spatiotemporally controlled gene delivery. *J Biomed Nanotechnol*. 2018;14(7):1287–1297. doi:10.1166/jbn.2018.2575
34. Lee JL, Lo CW, Inserra C, et al. Ultrasound enhanced PEI-mediated gene delivery through increasing the intracellular calcium level and PKC-δ protein expression. *Pharm Res*. 2014;31:2354–2366. doi:10.1007/s11095-014-1332-4
35. Yu J, Chen Z, Yan F. Advances in mechanism studies on ultrasonic gene delivery at cellular level. *Prog Biophys Mol Biol*. 2019;142:1–9. doi:10.1016/j.pbiomolbio.2018.07.012
36. Condello S, Morgan CA, Nagdas S, et al. β-Catenin-regulated ALDH1A1 is a target in ovarian cancer spheroids. *Oncogene*. 2015;34:2297–2308. doi:10.1038/onc.2014.178
37. Manta S, Renault G, Delalande A, et al. Cationic microbubbles and antibiotic-free miniplasmid for sustained ultrasound-mediated transgene expression in liver. *J Control Release*. 2017;262:170–181. doi:10.1016/j.jconrel.2017.07.015